CONF-

Towards Predicting Weld Metal Microstructure from Fundamentals of Transport Phenomena**

K. Mundra, T. DebRoy, S. S. Babu, S. A. David‡ and A. J. Paul#

The Pennsylvania State University, PA.
‡Metals and Ceramic Division, Oak Ridge National Laboratory, Oak Ridge, TN.
#Concurrent Technologies Corporation, Johnstown, PA.

Abstract

Heat transfer and fluid flow during manual metal arc welding of low alloy steels were investigated by solving the equations of conservation of mass, momentum and energy in three dimensions. Calculated cooling rates were coupled with an existing phase transformation model to predict the microstructure in low alloy steel welds. The computed results were found to be in good agreement with the experimentally observed microstructures. The agreement indicates significant promise for predicting spatial distribution of weld metal microstructure from the fundamentals of transport phenomena.

DISCLAIMER

This report was prepared as an account of work sponsored by an agency of the United States Government. Neither the United States Government nor any agency thereof, nor any of their employees, makes any warranty, express or implied, or assumes any legal liability or responsibility for the accuracy, completeness, or usefulness of any information, apparatus, product, or process disclosed, or represents that its use would not infringe privately owned rights. Reference herein to any specific commercial product, process, or service by trade name, trademark, manufacturer, or otherwise does not necessarily constitute or imply its endorsement, recommendation, or favoring by the United States Government or any agency thereof. The views and opinions of authors expressed herein do not necessarily state or reflect those of the United States Government or any agency thereof.

"The submitted manuscript has been authored by a contractor of the U.S. Government under contract No. DE-AC05-84OR21400. Accordingly, the U.S. Government retains a nonexclusive, royalty-free license to publish or reproduce the published form of this contribution, or allow others to do so, for U.S. Government purposes."

** The authors are grateful to Dr. H. K. D. H. Bhadeshia, University Reader, Department of Materials Science and Metallurgy, University of Cambridge, UK for allowing the authors to use his computer program to predict the microstructures in steel welds. The work was supported by the U.S. Department of Energy, Office of Basic Energy Sciences, Division of Materials Science, under grant numbers DE-FG02-84ER45158 with Pennsylvania State University and DE-AC05-84OR21400 with Martin Marietta Energy Systems, Inc.

DISTRIBUTION OF THIS DOCUMENT IS UNLIMITED

MASTER

DISCLAIMER

Portions of this document may be illegible in electronic image products. Images are produced from the best available original document.

Introduction

The integrity and the performance of a welded joint depend on the weldment microstructure and properties [1,2]. During welding, the interaction of the heat source and the material leads to rapid heating, melting and vigorous circulation of the molten material in the weld pool. As the heat source moves away from the molten region, solidification of the material takes place. The resulting thermal cycle plays an important role in determining the weldment structure and properties.

An accurate prediction of the thermal cycle in the weldment is a prerequisite for the prediction of weld metal microstructures in various regions of the weldment. Direct accurate measurements of temperature profiles in a weld pool are difficult. Furthermore, noncontact techniques for the measurement of temperature profiles in the weld pool are still evolving [3]. Earlier models to calculate temperature time-history in the welds were based on the solution of conservation of energy [4-6] and neglected the effect of fluid flow in the weld pool. Fluid flow in the weld pool may affect the time-temperature history experienced by a weld metal.

In the past decade, significant progress has been made in the solution of equations describing conservation of mass, momentum and energy in the weld pool [7-12]. The role of Marangoni, electromagnetic and the buoyancy forces on the weld pool geometry has been investigated [7,8]. The effect of surface active elements on the transient development of weld pool geometry has also been examined in details [13]. Simple features of solidification structure such as secondary dendrite arm spacing have been predicted from the cooling rate data calculated from fundamentals of transport phenomena [9]. These developments have provided significant insight into the welding process. However, accurate transient temperature calculations from comprehensive fluid flow and heat transfer models have not been used to predict fusion zone microstructures. The work reported here was aimed at predicting weld metal microstructures using detailed three dimensional transient temperature calculations from a heat transfer and fluid flow model in the weld pool and phase transformation theories of low alloy steels.

Model Framework

Fluid Flow and Heat Transfer in the Weld Pool

Since the quality of the weld metal microstructure calculations depends on the accuracy of the time-temperature history, the equations of conservation of mass, momentum and energy were solved in three dimensional forms. The welding process is transient when viewed in a stationary coordinate system (x,y,z). This transient problem can be transformed to a steady state problem by solving in a coordinate system that moves with the heat source (ξ,y,z). The details of the transformation of transient equations of mass, momentum, and energy conservation in the x,y,z coordinate system to the ξ,y,z coordinate system will be published elsewhere [14]. However, the final equations are given below.

Equation of Continuity

$$\nabla . \mathbf{V} = 0 \qquad (1)$$

where V is the velocity vector and U, V and W are the x, y and z component of the velocity vector, respectively. The material density, ρ, is assumed to be constant.

Momentum Equations

$$\rho \nabla (\mathbf{V}.\mathbf{V}) = -\nabla P + \mu \nabla .(\nabla \mathbf{V}) + \left(S_v - \rho \nabla .(\mathbf{V}_s \mathbf{V})\right) \qquad (2)$$

where V_s is the scanning velocity, μ is the viscosity, P is the effective pressure and S_v is the source term that takes into account the combined effect of buoyancy force, F_b, Marangoni stress, τ, and electromagnetic force, F_e.

Energy Equation

The technique used here to account for the phase change, has evolved from the work of Voller and Prakash [15]. The total enthalpy of the material, H, is represented as a sum of sensible heat, $h = \int C_p dT$, and latent heat content, ΔH. The energy equation is written in terms of the sensible heat, h, as follows:

$$\rho\nabla.(Vh) = \nabla.\left(\frac{k}{C_p}\nabla h\right) + S_l + S_h - \rho\nabla.(V_s h) \qquad (3)$$

where C_p is specific heat, k is thermal conductivity, S_h is the source term that takes into account the heat input from the welding source and the convective and radiative heat loss and S_l is the source term that accounts for latent heat of melting and convective transport of latent heat and is given by [15] :

$$S_l = \rho\nabla.(V\Delta H) + \rho\nabla.(V_s\Delta H) \qquad (4)$$

where $\Delta H = F(T)$, the latent heat content, is defined as a function of the temperature and is given by:

$$F(T) = L\left(\frac{T - T_s}{T_l - T_s}\right) \text{ for } T_s \le T \le T_l,\ F(T) = L \text{ for } T > T_l \text{ and } F(T) = 0 \text{ for } T < T_l \qquad (5)$$

where L is the latent heat, T_l is the liquidus temperature and T_s is the solidus temperature.

Boundary Conditions and Source Terms

The calculations were done only for half of the work piece, since there is a symmetry about y=0 plane. Along the plane of symmetry, V and the gradients of U and W were defined as zero. Since the weld pool surface was assumed to be flat, W was defined to be zero at the top surface. The condition that the velocity is zero in the mushy region is accounted by making use of enthalpy-porosity technique [15]. Assuming the Boussinesq treatment to be valid, density is assumed constant. The natural convection effect is taken into account by defining the buoyancy source term, S_b, to be:

$$S_b = \rho g\beta(T - T_{ref}) \qquad (6)$$

where β is the thermal expansion coefficient of liquid and T_{ref} is the reference temperature.

Since the temperature varies on the surface of the weld pool, a shear stress (Marangoni stress) is produced on the free surface. The effective tangential stress, τ, due to this effect on the free surface was calculated as follows:

$$\tau = f_l \frac{d\gamma}{dT}\nabla T \qquad (7)$$

where $d\gamma/dT$ is temperature coefficient of surface tension and f_l is the liquid fraction. The f_l is calculated from a relationship similar to the one presented in equation (5). The multiplication of the shear stress with f_l takes into account the decrease in the shear stress in the mushy region. The source term, S_e, was calculated by the formulation given by Kou et al. [10].

The source term for enthalpy equation, S_h, considered the heat exchange between the surface of the sample and the heat source including the radiative and convective heat loss to the surrounding [16]. Along the plane of symmetry, the gradient of enthalpy was zero. At the other surfaces of the sample, the temperature was prescribed as the interpass temperature.

The governing equations were represented in a finite difference form and solved iteratively on a line-by-line basis using Tri-Diagonal Matrix Algorithm (TDMA). The Semi-Implicit Method for Pressure-Linked Equations (SIMPLE) algorithm was employed for the discreatization of the equations. The details of the procedure are described elsewhere [17]. The model used 65 X 39 X 17 spatially non-uniform grids for the calculation of enthalpy and velocity.

Calculation of Temperature-Time Data

From the steady state temperature field, obtained by the solution of transformed momentum and enthalpy equation, temperature as a function of time at different locations (x,y,z) can be calculated by the following relation:

$$T(x,y,z,t2) = \frac{T(\xi 2,y,z) - T(\xi 1,y,z)}{\xi 2 - \xi 1} V_s(t2 - t1) + T(x,y,z,t1) \qquad (8)$$

where $T(\xi 2,y,z)$ and $T(\xi 1,y,z)$ are the steady state temperatures at coordinates $(\xi 2,y,z)$ and $(\xi 1,y,z)$, respectively, $(\xi 2 - \xi 1)$ is the distance traveled by the arc in time (t2 - t1), T(x,y,z,t1) and T(x,y,z,t2) are the temperatures at location (x,y,z) at times t1 and t2, respectively.

Phase Transformation Model

The low alloy steel weld metal microstructure consists of various ferrite morphologies such as allotriomorphic ferrite, Widmanstätten ferrite and acicular ferrite. The model developed by Bhadeshia et al. [18] is capable of predicting volume percentage of above ferrite morphologies for a given weld metal composition and welding process variables. This model calculates the paraequilibrium phase boundaries, CCT (continuous cooling transformation) diagrams using fundamentals of phase transformation theories of low alloy steels. The above calculations are then used to predict the volume percentage of ferrite morphologies. However, Bhadeshia et al. [18] used a semi-empirical approach to calculate the cooling rates in the fusion zone. In this work the cooling rates calculated from the solution of equations of conservation of mass, momentum and energy are coupled with the phase transformation model developed by Bhadeshia et al. [18] to predict the microstructure in the fusion zone.

Experimentation

The coupled fluid flow, heat transfer and microstructure model described above was used to predict microstructures for the experimental conditions published by Evans [19]. Evans has measured the volume fractions of ferrite morphologies in the top bead of multi-pass welds with different levels of V and Mn contents in Fe-C-Si low alloy steel welds. These weld beads were deposited by manual metal arc welding process with following conditions: welding voltage 21 V, welding current 170 A, welding speed 0.0027 m/s, and interpass temperature of 473 K. The weld joint geometry was in accordance with ISO 2560 joint [19]. For the above conditions,

thermal histories at different locations in the weldment were predicted using the fluid flow and heat transfer model. Application of the fluid flow and heat transfer model to manual metal arc welding will be discussed in the next section. The calculated cooling rates and the experimental austenite grain size data [19] were then used to calculate the microstructure within the fusion zone.

Results and Discussions

Fluid Flow and Heat Transfer

The three dimensional steady state temperature field obtained by the solution of the equations of conservation of mass, momentum and energy, for the welding condition of Evans [19], is shown in Figure 1. In the calculation of temperature field, the energy distributions from the arc and other sources such as metal droplets from the electrode, were coupled together and expressed in the form of an overall energy transfer efficiency. In view of the transport of large number of metal droplets during welding, time average values of the energy transport, implicit in our formulation, is thought to be justified. The complexity of the physical processes in the manual metal arc welding may, in fact, require adjustments of energy density distribution during the numerical simulation. Our assessment of this effect, considering different energy distribution, resulted in different peak temperatures and minor change in the weld pool geometry. However, no significant difference in temperature-time history was observed in the range of 1100 to 700 K. The temperature time history in the range of 1100 to 700 K governs the microstructural development in low alloy steel weldments. Moreover, the weld pool size was found to be similar to the experimental results of Evans [19]. Therefore, the application of the fluid flow and heat transfer model to the manual metal arc welding process is justified.

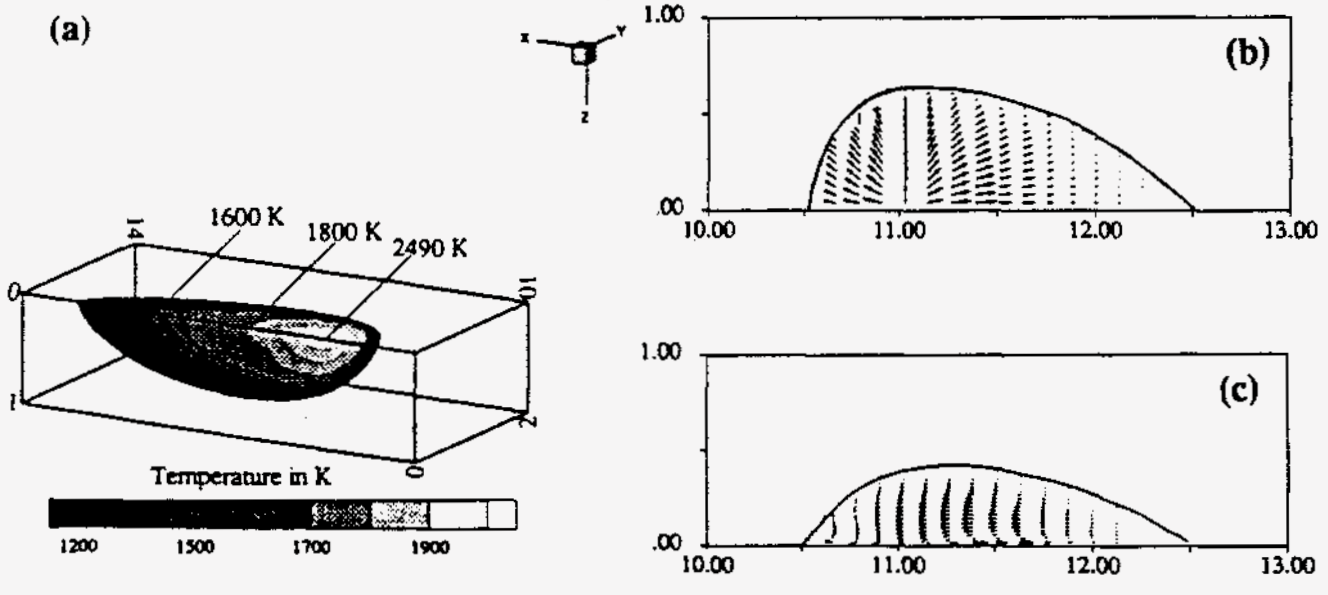

Fig 1. Calculated results: (a) three dimensional temperature distribution and velocity vectors on (b) top surface, and (c) along the plane of symmetry. Sample dimensions are in cm.

The temperature field shows a typical elongated weld pool. The peak temperature attained by the weld pool surface just below the arc was found to be 2490 K. In front of the heat source, the temperature gradient is much higher than that behind the heat source. This resulted in higher fluid velocities in front of the heat source. The temperature-time histories at (a) weld centerline on the surface of the weld, (b) mushy (solid-liquid) zone, (c) an intermediate posi-

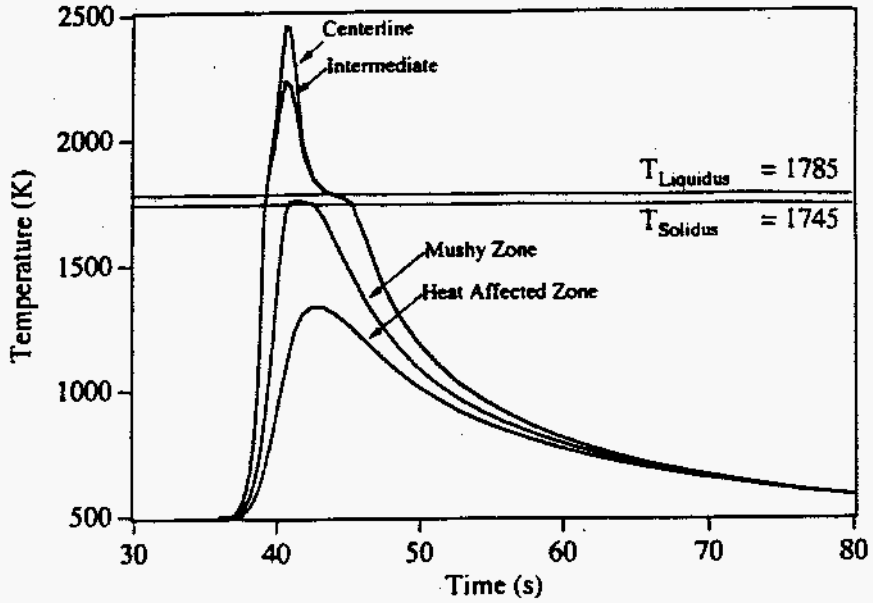

Fig 2. Temperature-time histories at different locations within the sample. Liquidus and solidus temperatures are also shown in the diagram.

tion between the weld centerline and mushy zone and in (d) heat affected zone are shown in Figure 2. These results show that cooling rates, given by the slope of the curves, are different at different locations.

Microstructural Calculation

Microstructural development in low alloy steel welds depends on the austenite to ferrite transformation kinetics and cooling rates experienced by the weld metal in the temperature range of 1100 to 700 K. To describe the cooling rates in the above temperature range, Svensson et al. [20] used a semi-empirical approach. Svensson and co-workers measured the cooling rates, experimentally, by harpooning Pt, Pt-Rh thermocouples into the weld pool region. Then, they fitted the experimentally measured cooling rates to the following equation:

$$\frac{dT}{dt} = \frac{C_1 (T - T_i)^{C_2}}{q\eta} \qquad (9)$$

where C_1 and C_2 are adjustable constants, T is the temperature of interest, T_i is the interpass temperature, q is the net welding heat input per unit length and η is the process efficiency. The above method assumed that the constants C_1 and C_2 to be independent of welding conditions and locations within the weld pool for a given welding process. Later on the equation (9) was used in the prediction of weld metal microstructure [18,20]. The above method may not be valid in all conditions and cannot be used for predicting the microstructural distribution as a function of location within the weld pool. However, the present work is capable of describing the cooling rates as a function of position within the weld pool. Figure 3 shows the cooling rates predicted by the present work as a function of temperature at various locations. The cooling rates differ to a certain degree. The cooling rates experienced at weld centerline and at intermediate location are higher than the cooling rates experienced in the mushy zone. In contrast, the model by Svensson et al. [20] predicts a unique cooling rate variation.

The cooling rates predicted by the present work are used in calculating the volume percentages of ferrite morphologies in the fusion zone for various Fe-C-Mn-V steel weld compositions

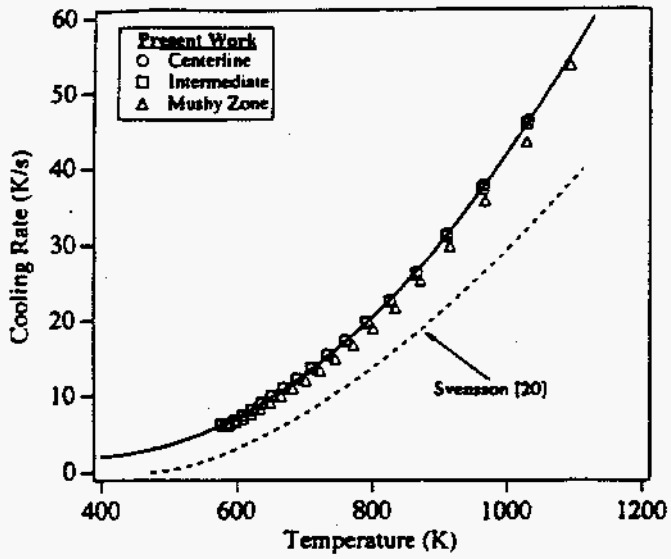

Fig 3. Cooling rates experienced at different locations within the weld pool. The cooling rates predicted by Svensson et al.[20] model is shown for comparison

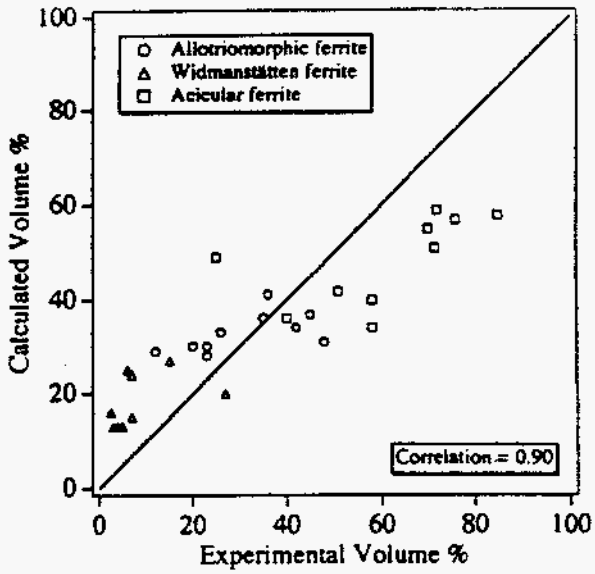

Fig 4. Comparison of calculated volume fractions of ferrite morphologies with the experimental values published by Evans [19].

given by Evans [19]. The calculations showed no significant difference in the microstructural constituents at different locations within the fusion zone. The calculated microstructural constituents in the intermediate zone are compared with the experimentally observed values in Fig. 4. The comparison shows a good correlation between the experimental observation and the calculated values and demonstrates the validity of the present work.

The above analysis showed no difference in the microstructural constituents at different locations due to a small change in the calculated cooling rate. However, in some high alloyed steels such as Fe-C-Cr-Mo welds, a small change in the cooling rates may lead to a different microstructural development [21]. This is illustrated with an example. The cooling rate calculations at various locations were applied to Fe-C-Cr-Mo (wt.%) weld. The results are presented in Table 1. It has been reported that in cases where allotriomorphic ferrite formation is completely suppressed (e.g. at weld centerline and intermediate region), the acicular ferrite microstructure may be replaced by bainitic microstructure [21]. The bainitic microstructure is deleterious to the weld metal properties and must be avoided. However, by allowing small amount of allotriomorphic ferrite formation, bainitic microstructure development can be suppressed and acicular ferrite microstructure can be promoted which leads to strong and tough welds. Hence, in the above example the weld properties at weld centerline and intermediate regions will be

Table 1. Calculated microstructural constitutions at different locations within the weld pool for Fe-0.07C-0.45Si-1.0Mn-0.5Ni-1.0Mo-2.25Cr (wt.%) weld.

Location	Ferrite Volume %		
	Allotriomorphic	Widmanstätten	Acicular
Centerline	0	0	100†
Intermediate	0	0	100†
Mushy Zone	11	5	84

†In these cases, the microstructure consists of mixture of acicular ferrite, bainite and martensite.

inferior to the weld properties at the mushy zone. The above results demonstrate that the present work can be used to predict the microstructural distribution within the fusion zone as a function of position and also in determining the crucial changes in microstructure development.

Summary and Conclusions

A numerical computational model to describe the heat transfer and fluid flow in welds has been developed. The fluid flow and heat transfer model predicted a small variation in the cooling rates at different locations within the fusion zone. The heat transfer and fluid flow model was coupled with an existing phase transformation model to describe the microstructure development in Fe-C-Mn-V low alloy steel welds. The computed microstructural results are found to be in good agreement with the experimentally observed microstructure. This agreement indicates significant promise for predicting the spatial weld metal microstructure distribution by coupling the fundamentals of transport phenomena with the phase transformation models.

References

1. S. A. David and T. DebRoy, Science, 257 (1992), 497-502.

2. T. DebRoy and S. A. David, in Reviews of Modern Physics, January 1995 (in press).

3. H. G. Kraus, Weld. J, 68 (1989), 269s.

4. D. Rosenthal, Trans. ASME, 68 (1946), 829.

5. C. M. Adams. Jr., Weld. J, 37 (1958), 211s-215s.

6. E. Friedman, Trans. ASME J. Pressure Vessel Techn., 97 Series J (3) (1975), 206-213.

7. G. M. Oreper and J. Szekely, Journal of Fluid Mechanics, 147 (1984), 53-79.

8. C. Chan, J. Mazumder and M. M. Chen, Metall. Trans A, 15A (1985), 2175-2184.

9. A. Paul, and T. DebRoy, Metall. Trans B, 19B (1988), 851-858.

10. S. Kou, and Y. H. Wang, Metall. Trans A, 17A (1986), 2265-2270.

11. T. Zacharia, S. A. David, J. M. Vitek and T. DebRoy, Weld. J., 68 (1989), 499-509s.

12. T. Zacharia, S. A. David, J. M. Vitek and T. DebRoy, Weld. J, 68 (1989), 510-519s.

13.W. Pitscheneder, T. DebRoy, K. Mundra, and R. Ebner, Submitted to Weld. J, 1994.

14. K. Mundra and T. DebRoy, 1994 Unpublished work, The Pennsylvania State University.

15. V. R. Voller, and C. Prakash, Intl. J. Heat Mass Transfer, 30 (1987), 1709-1719.

16. K. Mundra and T. DebRoy, Metall. Trans B, 24B (1993), 145-155.

17. S. V. Patankar, Numerical Heat Transfer and Fluid Flow (N. Y.: Hemisphere Publication Corp, 1980)

18. H. K. D. H. Bhadeshia, L. E. Svensson and B. Gretoft, Acta. Metall., 33 (1985), 1271.

19. G. M. Evans, OERLIKON-Schweißmitt, 49 (1991), 18-33.

20. L. E. Svensson, B. Gretoft and H. K. D. H. Bhadeshia, Scand. J. of Metall. 15 (1986), 96.

21. S. S. Babu and H. K. D. H. Bhadeshia, Mater. Sci. and Technol., 6 (1990), 1005-1020.